Measurement of $|V_{cb}|$ using the semileptonic decay $\overline{B}^0_d \to D^{*+}\ell^-\overline{\nu}_\ell$.

A. Oyanguren[1], P. Roudeau[2] and J. Salt[1]

(1) IFIC, Valencia-CSIC, and D.F.A.M.N., U. de Valencia

(2) U. de Paris-Sud, Lab. de l'Accélérateur Linéaire (L.A.L.), Orsay

Abstract

Events originating from the decay channel $\overline{B}^0_d \to D^{*+}\ell^-\overline{\nu}_\ell$, with $\ell = e$ or μ, in which the D^{*+} decay final state is exclusively reconstructed into $D^0\pi^+$ with $D^0 \to K^-\pi^+$ or $K^-\pi^+\pi^+\pi^-$, have been isolated by the DELPHI Collaboration in hadronic Z decays. These events are used to measure the CKM matrix element $|V_{cb}|$ and the slope of the ISGW form factor:

$$\mathcal{F}_{D^*}(1)\,|V_{cb}| = 0.0357 \pm 0.0024 \pm 0.0019; \quad \rho^2_{A_1} = 1.23 \pm 0.21 \pm 0.32$$

which correspond to a branching fraction: $BR(\overline{B}^0_d \to D^{*+}\ell^-\overline{\nu}_\ell) = (5.15 \pm 0.28 \pm 0.27)\%$

1 Introduction.

The Cabibbo, Kobayashi and Maskawa (CKM) matrix element V_{cb} is a parameter of the Standard Model and its value needs to be fixed by experiments. This parameter determines the decay rate of b-hadrons as the value of $|V_{ub}|$, which governs the other possible charged weak decay of b quarks, contributes by only 1-2% to the total decay rate. The value of $|V_{cb}|$ cannot be measured directly and there are two decay processes for which theoretical uncertainties are expected to be under control: the inclusive semileptonic decay of b-hadrons corresponding to the $b \to c\ell^-\overline{\nu}_\ell$ transition and the exclusive decay channel $\overline{B^0_d} \to D^{*+}\ell^-\overline{\nu}_\ell$. The latter is used in the following analysis, the D^{*+} is reconstructed through its cascade decay $D^0\pi^+$ and the D^0 meson is isolated using two decay channels: $K^-\pi^+$ and $K^-\pi^+\pi^+\pi^-$.

This study benefits from the reprocessing of DELPHI data registered between 1992 and 1995 through improved versions of the event reconstruction algorithms. As a consequence, the signal events statistics has increased by more than a factor two as compared with the previous publication [1] using the same decay final states. Improvements have been obtained also on the D^* mass and b-meson energy reconstruction. The D^{*+} signal being narrower, this gives a better isolation of the signal over the combinatorial background. As the main source of experimental systematic uncertainty originates from the contribution of D^{*+} mesons emitted in the decay of excited charmed states produced in b-hadron semileptonic decays, additional observables have been defined to control the level of this contamination in a better way.

2 Measurement of $|V_{cb}|$ from the decay $\overline{B^0_d} \to D^{*+}\ell^-\overline{\nu}_\ell$

The value of $|V_{cb}|$ is extracted by studying the decay partial width for the process $\overline{B^0_d} \to D^{*+}\ell^-\overline{\nu}_\ell$ as a function of the recoil kinematics of the D^{*+} meson. The decay rate is parameterized as a function of the variable w, defined as the product of the four-velocities of the D^{*+} and $\overline{B^0_d}$ mesons. This variable is related to the square of the four-momentum transfer from the $\overline{B^0_d}$ to the $\ell^-\overline{\nu}_\ell$ system, q^2, by:

$$w = \frac{m^2_{D^{*+}} + m^2_{B^0_d} - q^2}{2m_{B^0_d}m_{D^{*+}}}, \tag{1}$$

and its values range from 1.0, when the D^{*+} is produced at rest in the $\overline{B^0_d}$ rest frame, to about 1.50. Using HQET, the differential partial width for this decay is given by:

$$\frac{d\Gamma}{dw} = \frac{G^2_F |V_{cb}|^2}{48\pi^3}\mathcal{K}(w)\mathcal{F}^2_{D^*}(w) \tag{2}$$

where $\mathcal{K}(w)$ contains kinematic factors and $\mathcal{F}_{D^*}(w)$ is the hadronic form factor for the decay.

$$\mathcal{K}(w) = m^3_{D^*}(m_B - m_{D^*})^2\sqrt{w^2 - 1}(w + 1)^2\left(1 + \frac{4w}{w + 1}\frac{1 - 2wr + r^2}{(1 - r)^2}\right) \tag{3}$$

with $r = m_{D^*}/m_B$.

Although the shape of the form factor, $\mathcal{F}_{D^*}(w)$, is not known, its magnitude at zero recoil, corresponding to $w = 1$, can be estimated using HQET. It is found to be convenient to express $\mathcal{F}_{D^*}(w)$ in terms of the axial form factor $h_{A_1}(w)$ and of the reduced helicity form factors $\tilde{H}_0$ and $\tilde{H}_\pm$:

$$\mathcal{F}_{D^*}(w) = h_{A_1}(w) \sqrt{\frac{\tilde{H}_0^2 + \tilde{H}_+^2 + \tilde{H}_-^2}{1 + \frac{4w}{w+1} \frac{1 - 2wr + r^2}{(1-r)^2}}}. \tag{4}$$

The reduced helicity form factors are themselves expressed in terms of the ratios between the other HQET form factors ($h_V(w)$, $h_{A_2}(w)$, $h_{A_3}(w)$) and $h_{A_1}(w)$:

$$\tilde{H}_0(w) = 1 + \frac{w - 1}{1 - r}[1 - R_2(w)] \tag{5}$$

$$\tilde{H}_\pm(w) = \frac{\sqrt{1 - 2wr + r^2}}{1 - r}\left[1 \mp \sqrt{\frac{w - 1}{w + 1}} R_1(w)\right] \tag{6}$$

with

$$R_1(w) = \frac{h_V(w)}{h_{A_1}(w)} \text{ and } R_2(w) = \frac{h_{A_3}(w) + r h_{A_2}(w)}{h_{A_1}(w)}. \tag{7}$$

Values for $R_1(w)$ and $R_2(w)$ have been measured by CLEO [2] using different models.

The unknown function $h_{A_1}(w)$ is approximated with an expansion around $w = 1$ due to Caprini, Lellouch and Neubert (CLN) [3]:

$$h_{A_1}(w) = h_{A_1}(1) \times \left[1 - 8\rho_{A_1}^2 z + (53\rho_{A_1}^2 - 15)z^2 - (231\rho_{A_1}^2 - 91)z^3\right], \tag{8}$$

where $\rho_{A_1}^2$ is the slope parameter at zero recoil and $z = \frac{\sqrt{w+1} - \sqrt{2}}{\sqrt{w+1} + \sqrt{2}}$. An alternative parametrization, obtained earlier, can be found in [4].

In the heavy quark limit ($m_b \to \infty$), $\mathcal{F}_{D^*}(1) = h_{A_1}(1)$ coincides with the Isgur-Wise function [5, 6] which is normalized to unity at the point of zero recoil. Corrections to $\mathcal{F}_{D^*}(1)$ have been calculated to take into account the effects of finite quark masses and QCD corrections [7]. They yield $\mathcal{F}_{D^*}(1) = 0.91 \pm 0.04$.

Experiments determine the product $\mathcal{F}_{D^*}^2(1)|V_{cb}|^2$ by fitting this quantity and the slope $\rho_{A_1}^2$, using the expression (2), convoluted with the experimental resolution on the w variable. Since the phase space factor $\mathcal{K}(w)$ tends to zero as $w \to 1$, the decay rate vanishes at $w = 1$ and the accuracy of the extrapolation relies on achieving a reasonably constant reconstruction efficiency in the region close to $w = 1$.

3   Hadronic Event Selection and Simulation.

Hadronic Z decays registered by DELPHI between 1992 and 1995 have been analysed. Each event was divided into two opposite hemispheres by a plane othogonal to the thrust axis. To ensure that the event was well contained inside the fiducial volume of the detector, the polar angle of the thrust axis of the event had to satisfy the requirement $|\cos\theta| < 0.95$. Charged and neutral particles were clustered into jets by using the LUCLUS [8] algorithm with the resolution parameter $d_{join} = 5$ GeV.

About 3.4 million events were selected from the full LEP1 data sets. The JETSET 7.3 Parton Shower [8] program was used to generate hadronic Z decays, which were followed through the detailed detector simulation DELSIM [10] and finally processed by the same analysis chain as the real data. A sample of about nine million $Z \rightarrow q\overline{q}$ events was used. To increase the statistical significance of the simulation, an additional sample of about 3.6 million $Z \rightarrow b\overline{b}$ events was analysed, equivalent to about 17 million hadronic Z decays. Statistics of the analysed hadronic samples are given in Table 1.

Year	Real data	Simulated $Z \rightarrow q\overline{q}$	Simulated $Z \rightarrow b\overline{b}$
1992+1993	1355805	3916050	1096199
1994+1995	2012921	5012881	2495335
Total	3368726	8928931	3591534

Table 1: *Analysed number of events. In 1992 and 1993 only two-dimensional vertex reconstruction was available.*

D^0 mesons [1] have been reconstructed using their decays into $K^-\pi^+$ and $K^-\pi^+\pi^+\pi^-$. D^{*+} are measured using the $D^0\pi^+$ transition and the charged pion is denoted as π^* in the following.

4   Selection of the analysed events sample

Analysed events corresponding to candidates for the decay $\overline{B^0_d} \rightarrow D^{*+}\ell^-\overline{\nu}_\ell$ are selected by requiring the presence of an identified lepton and of a D^{*+} candidates in the same hemisphere. To reduce the contribution from Z decays into light flavours, the probability, given by the b-tagging algorithm, applied to the whole event, that the analysed event originates from light quarks is taken to be smaller than 0.5 and 0.1 when considering, respectively, the $D^0 \rightarrow K^-\pi^+$ and $\rightarrow K^-\pi^+\pi^+\pi^-$ decay channels. In addition, the mass of the $D^{*+} - \ell^-$ system is restricted to the range between 2.5 and 5.5 GeV/c^2.

4.1   Lepton identification

Muons and electrons, with a momentum larger than 2 GeV/c have been identified using the standard algorithms based on the matching of the track reconstructed in the tracking system to the track elements provided by the barrel and forward muon chambers. The loose selection criteria have been applied and the efficiency was $\sim 80\%$ for $\sim 1\%$ probability of hadron misidentification.

Electrons are identified using a neural network algorithm providing about 75% efficiency within the calorimeter acceptance. The probability for a hadron to fake an electron was about 1%. Electrons from photon conversions are mainly produced in the outer ID wall and in the inner TPC frame. About 80% of them were removed with negligible loss of signal by reconstructing their materialisation vertex.

---

[1]Throughout this paper charge-conjugate states are implicitly included.

4.2 Isolation of the $D^0 \to K^-\pi^+$ decay channel.

The kaon candidate corresponds to a particle of same charge as the lepton, with a momentum larger than 1 GeV/c and not identified as a pion by the standard algorithms which combine informations provided by the ionisation deposited in the gaz volume of the TPC and by RICH detectors. The pion candidate must have a charge opposite to the kaon charge and a momentum larger than 0.5 GeV/c. The pion and kaon candidates must be associated to, at least, one VD hit in $R\Phi$ and situated in the same event hemisphere as the lepton. The two tracks must intercept in space and only secondary D^0 vertices with a χ^2 probability larger than 10^{-3} have been retained. $K^-\pi^+$ systems of mass situated between 1.81 and 1.92 GeV/c^2 and with a momentum larger than 6 GeV/c are selected as signal candidates.

A D^0 track is reconstructed using the parameters of the K^- and π^+ tracks fitted at their common vertex and imposing the condition that the D^0 mass is equal to the value given in PDG [9]. The B decay vertex is obtained by intercepting the D^0 and the lepton trajectories. This vertex must have a χ^2 probability larger than 10^{-3} and only $D^0\ell^-$ pairs of total momentum larger than 10 GeV/c are kept. The B decay vertex is then required to be at a minimum distance from the position of the beam interaction point and a minimum distance is also required between the D and B measured decay points. These conditions, depend on the number of Z VD hits attached to the tracks. If the decay distance is not measured along Z with the VD, only cuts on decay distances transverse to the beam direction are applied. These requirements are rather loose, corresponding to a decay distance divided by its error larger than -2 to -1.

D^0 decay channel	92-93 MC	94-95 MC
$K^-\pi^+$	$(19.2 \pm 0.7)\%$	$(22.3 \pm 0.6)\%$
$K^-\pi^+\pi^+\pi^-$	$(8.6 \pm 0.3)\%$	$(10.8 \pm 0.3)\%$

Table 2: *Global efficiencies of the analysis chain to reconstruct and select signal simulated events. Quoted uncertainties are only of statistical origin.*

The D^{*+} signal is obtained by considering, in turn, all charged particles emitted in the same event hemisphere as the jet containing the lepton candidate and of charge opposite to the lepton charge. This track must form a vertex with the D^0 and the charged lepton trajectories and the vertex fit probability has to be higher than 10^{-3}. Signals for the cascade decay $D^{*+} \to D^0\pi^+$ correspond to a peak in the distribution of the mass difference $\delta_m = m(D^0\pi^+) - m(D^0)$.

The global efficiencies to select signal events (see Table 2), which include efficiencies of all analysis steps described above apart branching fractions of the D^{*+} and of the D^0 into the considered decay channels have been measured using simulated events.

4.3 Isolation of the $D^0 \to K^-\pi^+\pi^+\pi^-$ decay channel.

The kaon candidate corresponds to a particle of same charge as the lepton, with a momentum larger than 1 GeV/c and not identified as a pion by the standard algorithms, as in the previous analysed channel. Each of the three pion candidates must have a momentum
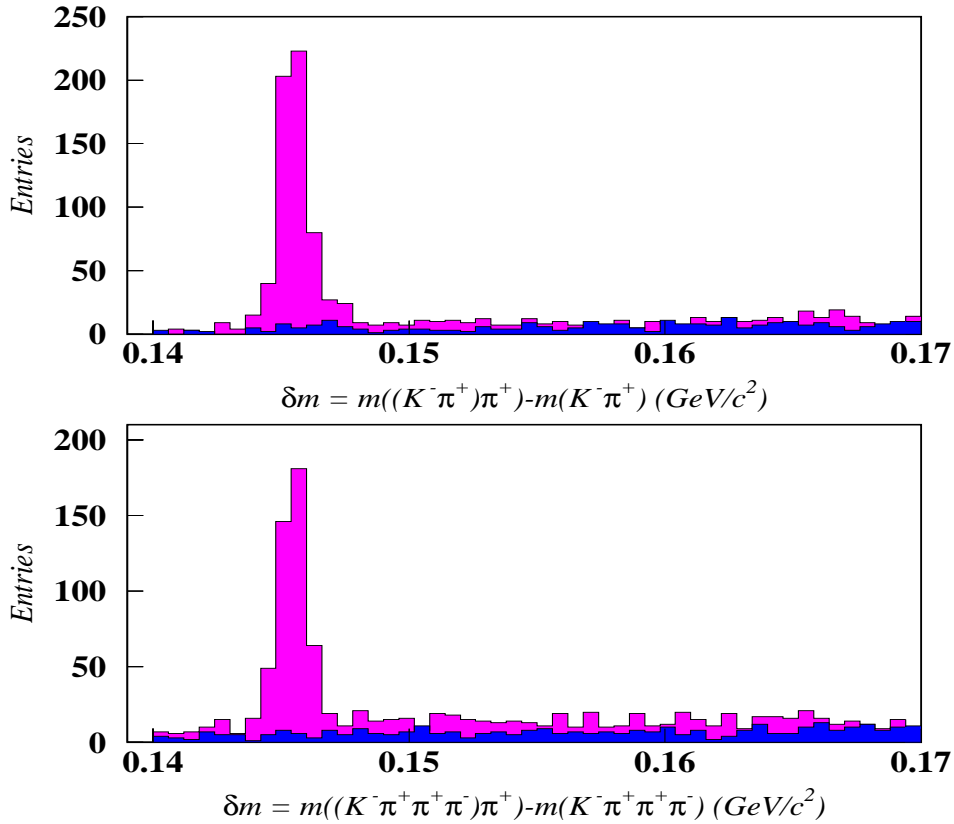
4

Figure 1: $\delta_m = m(D^0\pi^+) - m(D^0)$ *distributions for the* $D^0 \rightarrow K^-\pi^+$ *(upper plot)* *and* $D^0 \rightarrow K^-\pi^+\pi^+\pi^-$ *(lower plot) decay channels. Wrong-sign combinations are superimposed as darker histograms. Events registered in 92-93 and 94-95 have not been distinguished.*

larger than 0.5 GeV/c and the total charge of the three pion system has to be opposite to the kaon charge. At least two, among the four charged tracks candidates as D^0 decay products, must be associated to, at least, one VD hit in $R\Phi$ and be situated in the same event hemisphere as the lepton. The four tracks must intercept in space and only secondary D^0 vertices with a χ^2 probability larger than 10^{-3} have been retained. $K^-\pi^+\pi^+\pi^-$ systems of mass situated between 1.84 and 1.90 GeV/c^2 and with a momentum larger than 6 GeV/c are selected as signal candidates.

A D^0 track is formed using the parameters of the kaon and pions tracks fitted at their common vertex. The B decay vertex is obtained by intercepting the D^0 and the lepton trajectories. This vertex must have a χ^2 probability larger than 10^{-3} and only $D^0\ell^-$ pairs of total momentum larger than 10 GeV/c are kept. The B decay vertex is then required to be at a minimum distance from the position of the beam interaction point and a minimum distance is also required between the D and B decay points. These conditions, depend on the number of Z VD hits attached to the tracks. If the decay distance is not measured along Z with the VD, only cuts on decay distances transverse

to the beam direction are applied. Because of the higher combinatorial background, as compared with the $D^0 \to K^- \pi^+$ decay channel, these cuts are more severe than for the previous channel and are summarised in Table 3.

	B vert. $\Leftrightarrow$ main vert.	D vert. $\Leftrightarrow$ B vert
distance in space	$D/\sigma_D > 1$	$D/\sigma_D > -1$
transverse distance	$D/\sigma_D > 2$	$D/\sigma_D > -.5$

Table 3: *Minimum requirements on the decay distance (D) between the B and the main vertics and also between the D and the B vertices.*

The same set of four particles can give two $K^- \pi^+ \pi^+ \pi^-$ mass combinations if there is an ambiguity in the definition of the K^- and π^- candidates. Only one combination is kept in the analysis, using non-ambiguous signatures for these particles or, if this information is not available, considering that the K^- has the largest momentum.

The same selection criteria, as for the decay $D^0 \to K^- \pi^+$, are applied to search for a D^{*+} signal. Global efficiencies to select signal events (see Table 2), which include efficiencies of all analysis steps, apart branching fractions of the D^{*+} and of the D^0 into the considered decay channels, have been measured using simulated events.

4.4 Selected events candidates.

The mass difference distributions corresponding to the variable $\delta_m = m(D^0 \pi^+) - m(D^0)$ obtained for the two channels, are given in Figure 1.

The numbers of corresponding D^* candidates obtained by fitting these distributions with a Gaussian for the signal and a smooth distribution for the combinatorial background [2] are given in Table 4.

Data set	D^* cand.	$< m(D^*) - m(D^0) >$ MeV/c^2	$\sigma[m(D^*) - m(D^0)]$ MeV/c^2
$K^- \pi^+$ 92-93	193 ± 15	145.55 ± 0.05	0.63 ± 0.05
$K^- \pi^+$ 94-95	328 ± 16	145.47 ± 0.04	0.47 ± 0.04
$K^- \pi^+ \pi^+ \pi^-$ 92-93	144 ± 14	145.40 ± 0.07	0.63 ± 0.05
$K^- \pi^+ \pi^+ \pi^-$ 94-95	243 ± 17	145.49 ± 0.04	0.46 ± 0.03

Table 4: *Number of $D^* - \ell$ candidate events selected in the two data taking periods and for the two D^0 decay channels.*

4.5 q^2 measurement.

As explained in Section 2, to measure $|V_{cb}|$ it is necessary to study the q^2 dependence of the differential semileptonic decay partial width $d\Gamma(\overline{B}_d^0 \to D^{*+} \ell^- \overline{\nu}_\ell)/dq^2$. For signal

---

[2]The distribution considered for the combinatorial background is $b_m(\delta_m) = (\delta_m - m_\pi)^{a_{m,0}} \left(\sum_{k=1}^{n_m} a_{m,k} \delta_m^{k-1} \right)$, with $n_m = 2$ or 3 and $a_{m,0} = 0.5$.

events, corresponding to the semileptonic decay $\overline{\mathrm{B}}^0_\mathrm{d} \to \mathrm{D}^{*+}\ell^-\overline{\nu}_\ell$, the value of q^2 has been obtained from the measurements of the $\overline{\mathrm{B}}^0_\mathrm{d}$ and D^{*+} four-momenta:

$$q^2 = (p_\ell + p_{\overline{\nu}_\ell})^2 = (p_{\overline{\mathrm{B}}^0_\mathrm{d}} - p_{\mathrm{D}^{*+}})^2. \tag{9}$$

The D^{*+} 4-momentum is accurately measured, as all decay products correspond to reconstructed charged particle trajectories. To improve the determination of the $\overline{\mathrm{B}}^0_\mathrm{d}$ momentum, informations from all measured b-decay products are used, including the evaluation of the missing energy in the jet containing the lepton and the positions of the primary and of the secondary vertex which are used as constraints to define the direction of the b-hadron momentum. The nominal B^0_d mass is also used as a constraint. Finally, a momentum dependent correction is applied to the reconstructed b-hadron momentum so that it remains centreed on the generated value.

The smearing on the q^2 variable is studied on simulated signal events and a function $\mathcal{R}(q^2_s - q^2_r, q^2_s)$ is obtained which gives the distribution of the difference between the values of the reconstructed q^2, q^2_r, for events generated with a given value q^2_s (see Figure 2). Twenty slices in q^2_s of the same width have been considered. Within each slice, $\mathcal{R}(q^2_s - q^2_r, q^2_s)$ is parametrized as the sum of two Gaussian distributions. The two central positions of the Gaussians, their standard deviations and the fraction of events corresponding to the narrower Gaussian are parametrized with a linear dependence on q^2_s. Such parametrizations are obtained, independently, for two sets of ten slices. Typical values of these parametrisations correspond to q^2 resolutions of 0.3 and 2 GeV/c^2 with 30% of the events included in the narrower Gaussian.

The cuts applied to select the events which require a minimum momentum on the lepton, the D^{*+} and the $\mathrm{D}^{*+} - \ell$ system and the cut on the minimum value for the mass of the $\mathrm{D}^{*+} - \ell$ system can possibly introduce a bias in the q^2_s distribution. A q^2_s dependent acceptance correction, $\epsilon(q^2_s)$ has been evaluated by comparing the simulated q^2_s distributions, for signal events, before and after applying all analysis cuts. This correction has been normalized such that it does not change the number of accepted events for which an overall efficiency has been determined. The corresponding distribution is given in Figure 3. It is uniform and does not show evidence for any significant bias. A linear dependence for the acceptance gives:

$$\epsilon(q^2_s) = (0.983 \pm 0.030) \; + \; (0.0028 \pm 0.0049) \times q^2_s \tag{10}$$

which is compatible with unity within quoted uncertainties.

As the cuts used in the analysis are very similar for all data samples, the same q^2_s dependent acceptance correction has been used for all channels and data samples.

5 The analysis procedure

The purpose of this analysis is to determine the values of the parameters $\mathcal{F}_{D^*}(1)\,|\mathrm{V}_{cb}|$ and $\rho^2_{A_1}$, introduced in Section 2, using the measured q^2_r distribution of candidate events. The q^2_r distribution for the signal is obtained using the expected distribution from theory, corresponding to fixed values of the two parameters mentioned before, multiplied by the overall efficiency and the q^2_s dependent acceptance correction and convoluted with the expected resolution function $\mathcal{R}(q^2_s - q^2_r, q^2_s)$. The q^2_r distributions for the other events
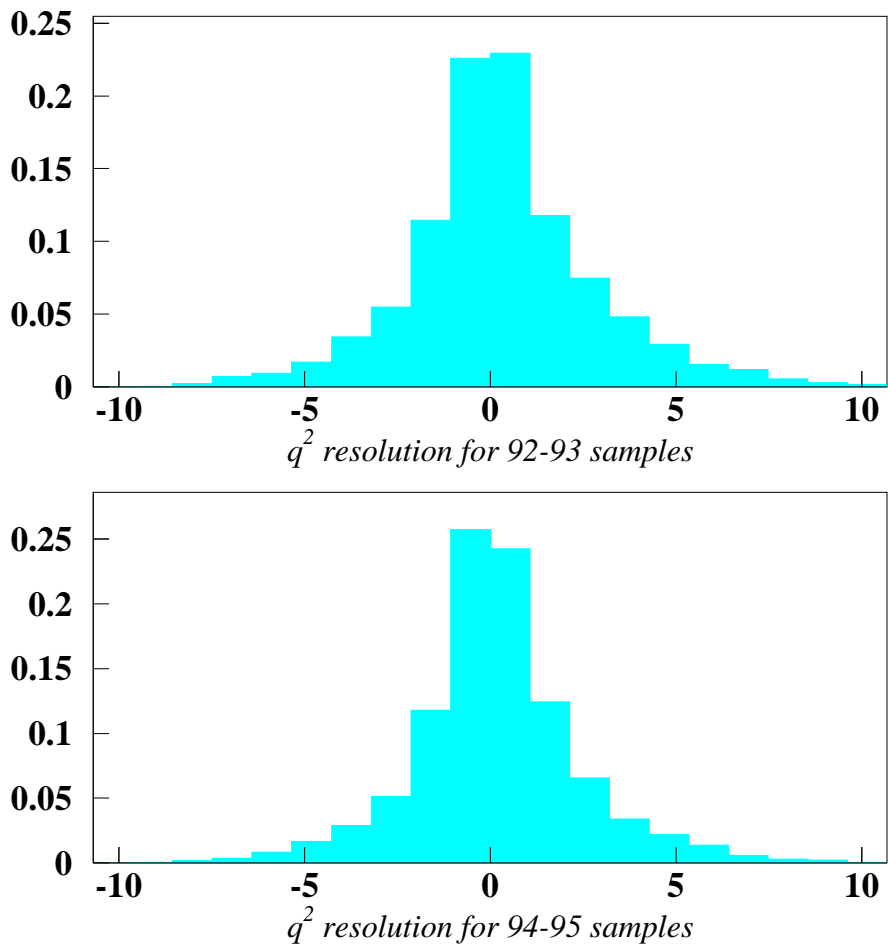
Figure 2: $\mathcal{R}(q_s^2 - q_r^2, q_s^2)$ for the two periods of data taking 92-93 and 94-95.
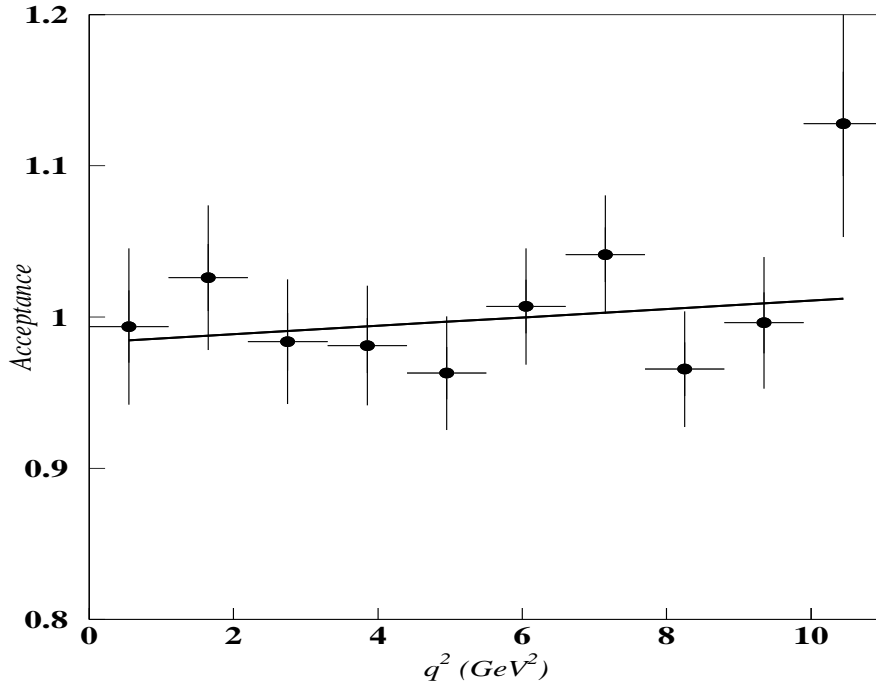
Figure 3: *Variation of the acceptance correction as a function of the value of the simulated q^2.*

sources are taken from the simulation or from real data in case of the combinatorial background. It happens that q_r^2 distributions are rather similar for the signal and other events categories. This comes from the procedure used to evaluate q_r^2, from the $\overline{\mathrm{B}_\mathrm{d}^0}$ and D^{*+} 4-momenta which overestimates the real q^2 value in case of background events. To enhance the separation between the signal and other events sources, two other variables have been used. Before describing these quantities, the different events classes contributing in the analysis have been listed.

5.1   The Event Sample composition

In addition to the signal (S1) which corresponds to the decay $\overline{\mathrm{B}_\mathrm{d}^0} \to \mathrm{D}^{*+}\ell^-\overline{\nu}_\ell$, there are six classes of events which contribute to the background.

- the combinatorial background (B) under the D^{*+} peak.

- real $\mathrm{D}^{*+} - \ell^-$ events with the D^{*+} produced in the decay of an excited charmed state (S2). These events correspond to the decay chain $b \to \mathrm{D}^{**}\ell^-\overline{\nu}_\ell$, $\mathrm{D}^{**} \to \mathrm{D}^{*+}\mathrm{X}$. By D^{**} are meant, in the present analysis, resonant as well as nonresonant excited $\mathrm{D}n\pi$ systems.

- real $\mathrm{D}^{*+} - \ell^-$ events with the lepton originating from the decay of another charmed hadron (S3).

9

- events in which the D*+ is emitted during the hadronization of a charmed quark jet in $Z \rightarrow c\bar{c}$ events (S4).

- $Z \rightarrow b\bar{b}$ events with a real D*+ candidate accompanied by a fake lepton of opposite sign (S5).

- real $D^{*+} - \ell^-$ events with the lepton originating from the decay of a τ^- lepton (S6).

5.2 Separation between signal and background events sources

There are two main classes of events corresponding respectively to events containing or not a real D*+. The variable δ_m allows to separate the two classes (see Figure 1).

To separate between the different classes of events, with a real D*+, the variables, $d_\pm$, are used. They are obtained from a measurement of the number of charged tracks, compatible with the b decay vertex, and of their compatibility with the main vertex, in addition to the charged lepton, the π^* and the D^0 decay products. For the signal, it is expected that all other charged particles in the b-jet are, apart for the $\overline{B}^0_d$ decay products, emitted from the beam interaction region. This will be also true for (S4), the remaining background from $Z \rightarrow c\bar{c}$ events, and for (S6). For the other classes (S2, S3 and S5) it is expected that, for most of the events, one or more charged particles are produced at the b-vertex in addition to those retained in the analysis.

The variables $d_\pm$ are defined in the following way:

- consider all charged particles emitted in the same event hemisphere as the b-candidate, which are different from the D*+ decay products and from the lepton, with a momentum larger than 500 MeV/c, which form a mass, adding the $D^{*+} - \ell^-$ system, lower than 6 GeV/c^2 and having values for their impact parameters, relative to the b decay vertex smaller than 2 and 1.5 σ in Rϕ and z respectively,

- count the number of candidates having the same (d_+) or the opposite (d_-) charge as the lepton,

- if there are several candidates, take the one with the largest impact parameter relative to the main vertex and evaluate the quantity:

$$x_\pm = \epsilon(\mathrm{R}\phi) \times nsig(\mathrm{R}\phi)^2 + \epsilon(z) \times nsig(z)^2 \qquad (11)$$

where, ϵ and $nsig$ are, respectively, the sign and the number of standard deviations for the track impact parameter relative to the main vertex

As the track offsets extend to very large values because of the exponential decay time of b-hadrons, the variable $d_\pm$ is taken to be equal to the logarithm of $(1 + x^2_\pm)$ and its sign is the same a x. For events with no spectator track candidate, a fixed value of -4. is given to $d_\pm$. Examples of distributions of the variable d_+ for the signal and the different background components, corresponding to the 94-95 period and to the $D^0 \rightarrow K^-\pi^+$ decay channel are given in Figure 4.
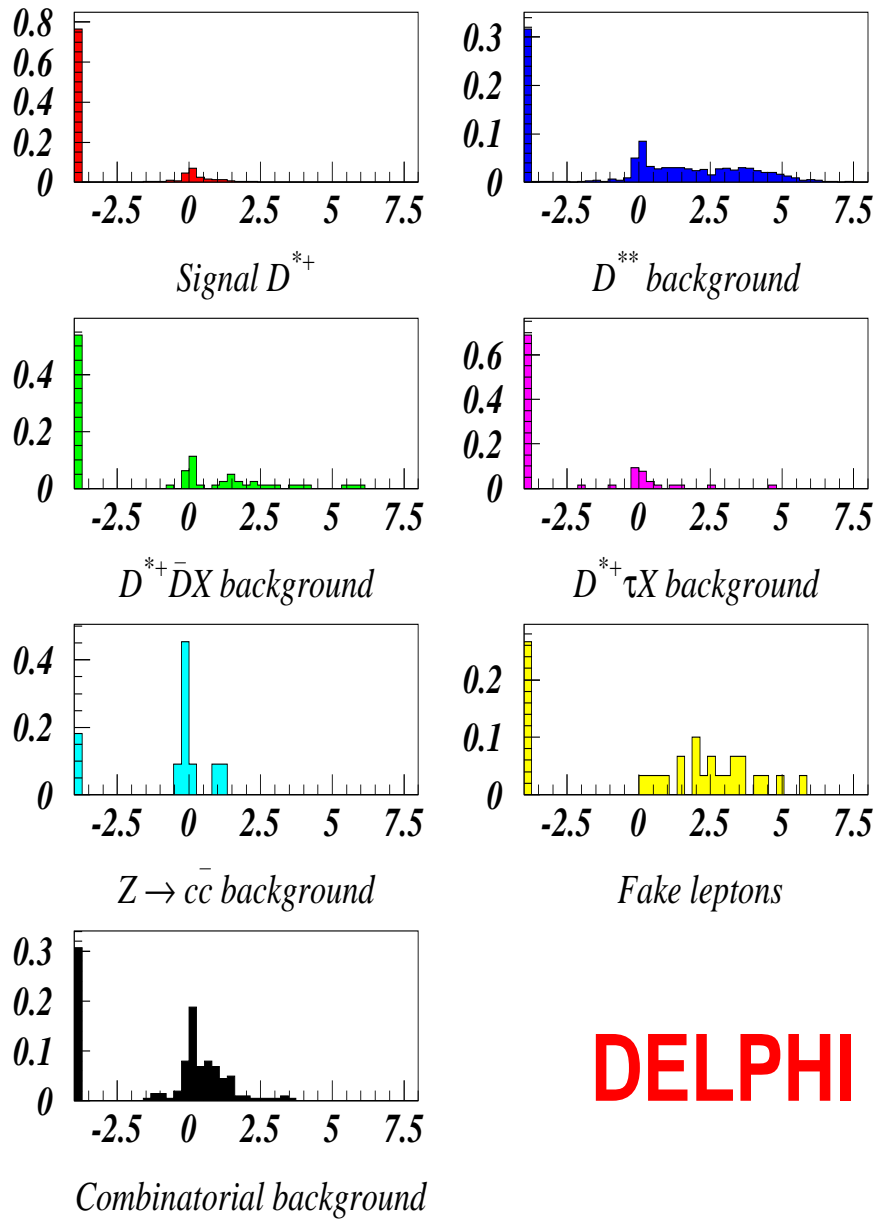
Figure 4: *Distributions of the d_+ variable for signal and background components. All distributions have been normalized to unity.*

5.3 Analysis procedures

Four events samples have been analysed separately as they correspond to different properties of the spectrometer (1992-1993 and 1994-1995) and to different decay channels of the D^0 ($K^-\pi^+$ and $K^-\pi^+\pi^+\pi^-$)

In the following, the analysis procedure is explained for one of these categories.

For each event (i), four measurements have been used: $\vec{x}_i = (q_r^2,\ \delta_m,\ d_+,\ d_-)_i$. The parameters $\mathcal{F}_{D^*}(1)|V_{cb}|$ and $\rho_{A_1}^2$ are obtained by minimizing a negative log-likelihood distribution. Other parameters have to be introduced to account for the various fractions of contributing events classes and to describe their behaviour in terms of the analysed variables. The likelihood distribution is obtained from the product of the probabilities to observe $\vec{x}_i$ for each considered event. These probabilities can be expressed in terms of the corresponding probabilities for each event's class and of their respective contributions in the analysed events samples:

$$\mathcal{P}(\vec{x}_i) = \frac{B \times b(\vec{x}_i) + \sum_{j=1}^{6} S_j \times s_j(\vec{x}_i)}{B + \sum_{j=1}^{6} S_j}. \tag{12}$$

In this expression, B and S_j, $(j = 1 - 6)$ are the numbers of events (fitted) corresponding to the combinatorial background and to the different classes of events with a real D^{*+}. The functions $b(\vec{x})$ and $s_j(\vec{x})$, $(j = 1 - 6)$ are the respective probability distributions of the variable $\vec{x}$. Each probability distribution for the $\vec{x}$ variable is considered to be the product of four probability distributions corresponding, respectively, to the different variables.

These distributions can be obtained from data $(b(\vec{x}))$ or from the simulation. The fitting procedure consists in minimizing the quantity:

$$-\ln\mathcal{L} = -\sum_{i=1}^{N_{evt}} \ln\mathcal{P}(\vec{x}_i) \tag{13}$$

where N_{evt} is the total number of analysed events.

From external measurements there are also constraints on the expected number of events corresponding to the categories S2-S6. These constraints can be applied assuming that the corresponding events numbers obey to Poisson distributions with fixed average values (S_j^0). This is obtained by adding to Equation (13) the quantity:

$$-\sum_{j=2}^{6} S_j \ln S_j^0 + \sum_{j=2}^{6} \ln\Gamma(S_j + 1) \tag{14}$$

A similar expression is also added to account for the fact that the total number of fitted events must be compatible with the number (N) of selected events:

$$-N_f \ln N + \ln\Gamma(N_f + 1) \tag{15}$$

in which N_f, the number of fitted events, is equal to: $N_f = \sum_{i=1,6} S_i + B$.

5.3.1 signal events

$s_{1,q_r^2}(q_r^2)$: this distribution results from the convolution of the theoretical expected distribution $\frac{d\Gamma(\overline{B}_d^0 \to D^{*+}\ell^-\overline{\nu}_\ell)}{dq_s^2}$, multiplied by the q_s^2 dependent efficiency function, with the

resolution function $\mathcal{R}(q_s^2 - q_r^2, q_s^2)$. It depends mainly on $\rho_{A_1}^2$ and on the assumed q_s^2 dependence for the ratio R_1 and R_2 between the different contributing form-factors.

$s_{1,\delta_m}(\delta_m)$: is a Gaussian distribution corresponding to the D^{*+} signal. Its central value and standard deviation are fitted on data.

$s_{1,d_\pm}(d_\pm)$: these distributions are obtained from simulated signal events. The two distributions, for d_+ and d_- variables are rather similar with about 80% probability for having no spectator track candidate and the remaining 20% being concentrated around zero.

S_1: the amount of signal events can be expressed as:

$$S_1 = N_H \times R_b \times 4 \times f_{\overline{\mathrm{B}_\mathrm{d}^0}} \times \mathrm{BR}(\overline{\mathrm{B}_\mathrm{d}^0} \to \mathrm{D}^{*+}\ell^-\overline{\nu}_\ell) \times \mathrm{BR}(\mathrm{D}^{*+} \to \mathrm{D}^0\pi^+) \times \mathrm{BR}(\mathrm{D}^0 \to \mathrm{X}) \times \epsilon(\mathrm{X}).$$
(16)

In this expression, N_H is the number of analysed hadronic events (Table 1), R_b is the fraction of hadronic Z decays into $b\overline{b}$ pairs, the factor 4 corresponds to the two jets and the fact that muons and electrons are used, $f_{\overline{\mathrm{B}_\mathrm{d}^0}}$ is the production fraction of $\overline{\mathrm{B}_\mathrm{d}^0}$ mesons in a b-quark jet, $\mathrm{BR}(\overline{\mathrm{B}_\mathrm{d}^0} \to \mathrm{D}^{*+}\ell^-\overline{\nu}_\ell)$ is the semileptonic branching fraction of $\overline{\mathrm{B}_\mathrm{d}^0}$ mesons which is measured in this analysis [3], the other two branching fractions correspond, respectively, to the selected D^{*+} and D^0 decay channels (Table 9), and $\epsilon(\mathrm{X})$ are the efficiencies, given in Table 2, of the cuts applied in the analysis to select signal events. One can note that S_1 is proportional to $(\mathcal{F}_{D^*}(1)\,|\mathrm{V}_{cb}|)^2$.

5.3.2   events from D** decays

These are events from the S2 class corresponding to the cascade decay $b \to \mathrm{D}^{**}\ell^-\overline{\nu}_\ell$, $\mathrm{D}^{**} \to \mathrm{D}^{*+}\mathrm{X}$.

$s_{2,q_r^2}(q_r^2)$: this distribution is taken from the simulation. Its variation for different fractions of D** states has been studied.

$s_{2,\delta_m}(\delta_m)$: the same distribution as for the signal, $s_{1,\delta_m}(\delta_m)$, is used

$s_{2,d_\pm}(d_\pm)$: as for the signal, these distributions are taken from the simulation. It has been verified that they are not dependent of the type of D** state which produced the D^{*+}. There is a marked difference between s_{2,d_+} and s_{2,d_-}, the latter being rather similar to the corresponding distribution for signal events.

S_2: the number of expected events is fitted without imposing constraints from external measurements.

5.3.3   cascade decay lepton events

These are events from the S3 class corresponding to the cascade decay $b \to \mathrm{D}^{*+}\overline{\mathrm{D}}\mathrm{X}$, $\overline{\mathrm{D}} \to \ell^-\overline{\nu}_\ell\mathrm{Y}$

$s_{3,q_r^2}(q_r^2)$: this distribution is taken from the simulation.

$s_{3,\delta_m}(\delta_m)$: the same distribution as for the signal, $s_{1,\delta_m}(\delta_m)$, is used

---

[3]It is the integral of Equation 2 and it depends on the two fitted quantities $\mathcal{F}_{D^*}(1)\,|\mathrm{V}_{cb}|$ and $\rho_{A_1}^2$.

$s_{3,d_\pm}(d_\pm)$: When there are spectator tracks, the distribution $s_{2,d_+}(d_+)$ (with $d_+ > -4$), is used. The expected fractions of events with no spectator tracks, in the d_+ and d_- distributions, have been evaluated from the measured contributions of $\overline{D}^0 D^{*+}$, $D^- D^{*+}$ and $D_s^- D^{*+}$ events [11], with the $\overline{D} \rightarrow \ell^- X$ branching fractions and topological decay rates for the hadronic states X, taken from [9].

S_3: the expected number of events from this source is taken from present measurements of $b \rightarrow D\overline{D}X$ decay rates which correspond to:

$$BR(b \rightarrow D^{*+}\ell^- X) + BR(b \rightarrow D^{*-}\ell^+ X) = (0.90 \pm 0.25)\%. \tag{17}$$

This value has been obtained using measurements [11] from ALEPH on exclusive double charm decay branching fractions of b-hadrons, with a charged D^* emitted in the final state, and using the inclusive semileptonic decay branching fractions of charmed particles given in [9].

Simulated events contain only double charm decays of the type $b \rightarrow D^{*+}D_s^{(*)}X$ with a corresponding branching fraction: $BR(b \rightarrow D^{*+}\ell^- X) = 0.25\%$. This rate has been rescaled to correspond to the value given in Equation (17), assuming that the experimental acceptance is similar for the different contributing channels.

5.3.4 $Z \rightarrow c\overline{c}$ events

$s_{4,q_r^2}(q_r^2)$: this distribution is taken from the simulation.

$s_{4,\delta_m}(\delta_m)$: the same distribution as for the signal, $s_{1,\delta_m}(\delta_m)$, is used

$s_{4,d_\pm}(d_\pm)$: as for the signal, it is taken from the simulation.

S_4: the expected number of events from this source is taken from the simulation after having corrected for the small difference between the rates for D^{*+} production in c-jets between simulated and real events:

$$P(c \rightarrow D^{*+}) = (0.2392 \pm 0.0035)_{MC} \leftrightarrow (0.226 \pm 0.014)_{Data} \tag{18}$$

5.3.5   fake lepton events

Only fake lepton events associated with a real D^{*+} have to be considered as the others are already included in the sample of combinatorial background events.

$s_{5,q_r^2}(q_r^2)$: this distribution is taken from the simulation.

$s_{5,\delta_m}(\delta_m)$: the same distribution as for the signal, $s_{1,\delta_m}(\delta_m)$, is used

$s_{5,d_\pm}(d_\pm)$: as for the signal, it is taken from the simulation.

S_5: the expected number of events from this source is taken from the simulation after having applied corrections determined, using special events samples, to account for differences between the fake lepton rates in real and simulated data (see Section 6.3).

5.3.6 combinatorial background events

Analysed events in real data are selected in the upper wing of the D^{*+} mass peak between 0.15 and 0.17 GeV/c^2.

$b_{q_r^2}(q_r^2)$: a polynomial behaviour is assumed for this distribution and the coefficients are fitted on data.

$b_{\delta_m}(\delta_m)$: the parametrisation given in Section 4.4 has been used and the same normalized mass distribution has been used in the four samples. Parameters of this distribution have been fitted on selected events for the analysis.

$b_{d_{\pm}}(d_{\pm})$: as for the mass distribution, the $d_{\pm}$ distributions for combinatorial background events are obtained from analysed events, selecting those situated in the upper part of the δ_m distribution.

B: in each of the four samples, the total number of combinatorial background events is fitted over the total δ_m range.

5.3.7 semileptonic decays with a τ

These are events from the S6 class corresponding to the cascade decay $b \rightarrow$ D$^{*+}\tau^- $X, $\tau^- \rightarrow \ell^- \overline{\nu}_\ell$Y

$s_{6,q_r^2}(q_r^2)$: this distribution is taken from the simulation.

$s_{6,\delta_m}(\delta_m)$: the same distribution as for the signal, $s_{1,\delta_m}(\delta_m)$, is used

$s_{6,d_{\pm}}(d_{\pm})$: is the same as the signal distribution $s_{1,d_{\pm}}(d_{\pm})$

S_6: the expected number of events from this source is obtained assuming that the production rate for b-hadron semileptonic decays is 0.223 ± 0.004 of the rate with a light lepton [12].

6 Measurements of $\mathcal{F}_{D^*}(1)\left|\mathrm{V}_{cb}\right|$ and $\rho^2_{A_1}$

The four events samples have been analysed in the same way. Efficiencies and probability distributions have been determined independently for the four samples. Common parameters corresponding to the description of physics processes have been fitted or taken from external measurements. Central values and uncertainties on these quantities, used in the analysis, have been summarised in Table 9.

6.1 Results on simulated events

Signal events generated using the DELPHI simulation program correspond to a given dynamical model using a given modelling of the decay form factors. The generated q^2 distribution has been fitted using a parametrization derived from the one given in Section 2. As the model used in the simulation is a priori different from HQET expectations, it has been necessary to add arbitrary terms in the expression so that the fit will be reasonable
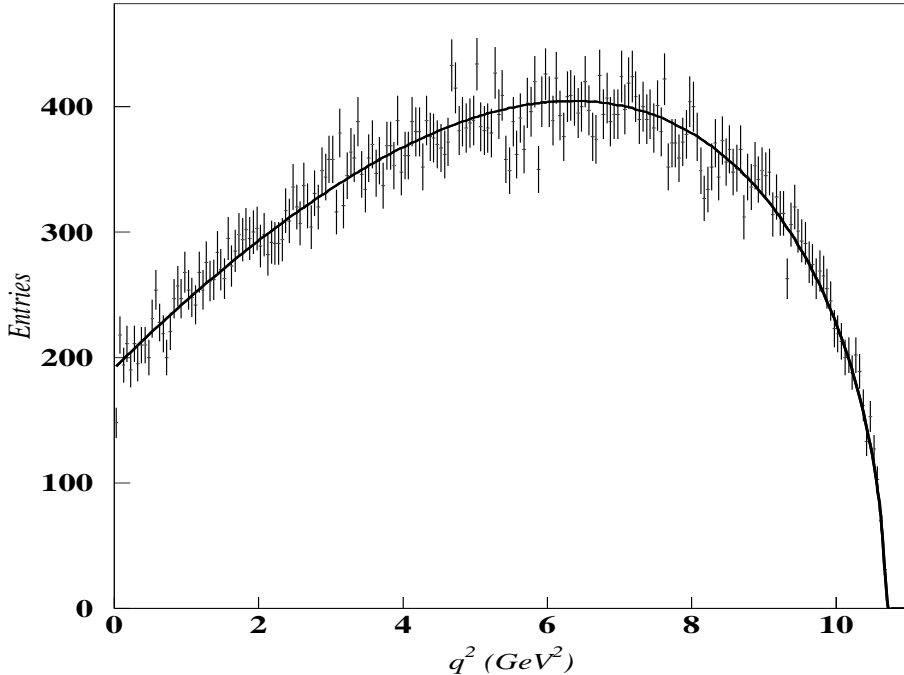
Figure 5: *Fit on pure signal simulated events. This spectrum corresponds to the DELPHI simulation with default parameters.*

over the whole q^2 variation range. These terms correspond to a polynomial development in powers of $(w-1)$, starting with at least quadratic terms so that they have no effect on the slope nor on the absolute value of the spectrum at the end-point corresponding to $w = 1$.

In addition, the constraint from the normalization has been included to obtain the equivalent values for the two parameters defining the signal in the simulation:

$$\mathcal{F}_{D^*}(1)\,|V_{cb}| = 0.03552 \pm 0.00016; \;\; \rho_{A_1}^2 = 1.088 \pm 0.021 \tag{19}$$

The fitted semileptonic branching fraction is equal to:

$$\mathrm{BR}(\overline{\mathrm{B}}_\mathrm{d}^0 \to \mathrm{D}^{*+}\ell^-\overline{\nu}_\ell) = (5.091 \pm 0.020)\% \tag{20}$$

which agrees with the exact value of 5.103% used to generate these events.

The exercise is repeated on pure signal events using the reconstructed q_r^2 distribution. The predicted distribution includes now the effects of the experimental reconstruction of the q^2 variable and of the acceptance.

$$\mathcal{F}_{D^*}(1)\,|V_{cb}| = 0.03561 \pm 0.00070; \;\; \rho_{A_1}^2 = 1.141 \pm 0.072 \tag{21}$$

The fitted semileptonic branching fraction is equal to:

$$\mathrm{BR}(\overline{\mathrm{B}}_\mathrm{d}^0 \to \mathrm{D}^{*+}\ell^-\overline{\nu}_\ell) = (4.980 \pm 0.069)\% \tag{22}$$

16

Finally, using the sample of $Z \to q\overline{q}$ and $b\overline{b}$ simulated events, the signal parameters are determined, including the different background components (see Table 5) giving:

$$\mathcal{F}_{D^*}(1)\,|\mathrm{V}_{cb}| = 0.03586 \pm 0.00079; \ \rho_{A_1}^2 = 1.106 \pm 0.076 \qquad (23)$$

The fitted semileptonic branching fraction is equal to:

$$\mathrm{BR}(\overline{\mathrm{B}}_{\mathrm{d}}^0 \to \mathrm{D}^{*+}\ell^-\overline{\nu}_\ell) = (5.141 \pm 0.084)\% \qquad (24)$$

Data set	$\mathcal{F}_{D^*}(1)\,|\mathrm{V}_{cb}|$	$\rho_{A_1}^2$	$\mathrm{BR}(\overline{\mathrm{B}}_{\mathrm{d}}^0 \to \mathrm{D}^{*+}\ell^-\overline{\nu}_\ell)$ (%)
$\mathrm{K}^-\pi^+$ 92-93	0.0388 ± 0.0020	1.37 ± 0.18	5.25 ± 0.21
$\mathrm{K}^-\pi^+$ 94-95	0.0346 ± 0.0013	1.04 ± 0.13	4.95 ± 0.14
$\mathrm{K}^-\pi^+\pi^+\pi^-$ 92-93	0.0374 ± 0.0021	1.20 ± 0.20	5.32 ± 0.23
$\mathrm{K}^-\pi^+\pi^+\pi^-$ 94-95	0.0353 ± 0.0013	1.02 ± 0.13	5.21 ± 0.15
Total sample	0.03586 ± 0.00079	1.106 ± 0.076	5.141 ± 0.084

Table 5: *Fitted values of the parameters on $Z \to q\overline{q} + b\overline{b}$ simulated events. Quoted uncertainties are only of statistical origin.*

6.2   Results on data

To analyse real data events additional corrections have been applied to account for remaining differences between real and simulated events. Central values and uncertainties on these corrections are explained in the following when evaluating systematic uncertainties attached to present measurements.

The results obtained on the four data samples and their average are given in Table 6.

Data set	$|\mathcal{F}_{D^*}(1)\,|\mathrm{V}_{cb}||$	$\rho_{A_1}^2$	$\mathrm{BR}(\overline{\mathrm{B}}_{\mathrm{d}}^0 \to \mathrm{D}^{*+}\ell^-\overline{\nu}_\ell)$ (%)
$\mathrm{K}^-\pi^+$ 92-93	0.0380 ± 0.0060	1.41 ± 0.47	5.28 ± 0.77
$\mathrm{K}^-\pi^+$ 94-95	0.0305 ± 0.0043	0.66 ± 0.49	5.07 ± 0.56
$\mathrm{K}^-\pi^+\pi^+\pi^-$ 92-93	0.0422 ± 0.0057	1.57 ± 0.41	5.93 ± 0.73
$\mathrm{K}^-\pi^+\pi^+\pi^-$ 94-95	0.0333 ± 0.0041	1.12 ± 0.40	4.76 ± 0.50
Total sample	0.0347 ± 0.0024	1.13 ± 0.23	5.14 ± 0.28

Table 6: *Fitted values of the parameters on real data events. Quoted uncertainties are only of statistical origin.*

These latter values are:

$$\mathcal{F}_{D^*}(1)\,|\mathrm{V}_{cb}| = 0.0347 \pm 0.0024; \ \rho_{A_1}^2 = 1.13 \pm 0.23 \qquad (25)$$

which correspond to a branching fraction equal to:

$$\mathrm{BR}(\overline{\mathrm{B}}_{\mathrm{d}}^0 \to \mathrm{D}^{*+}\ell^-\overline{\nu}_\ell) = (5.14 \pm 0.28)\% \qquad (26)$$
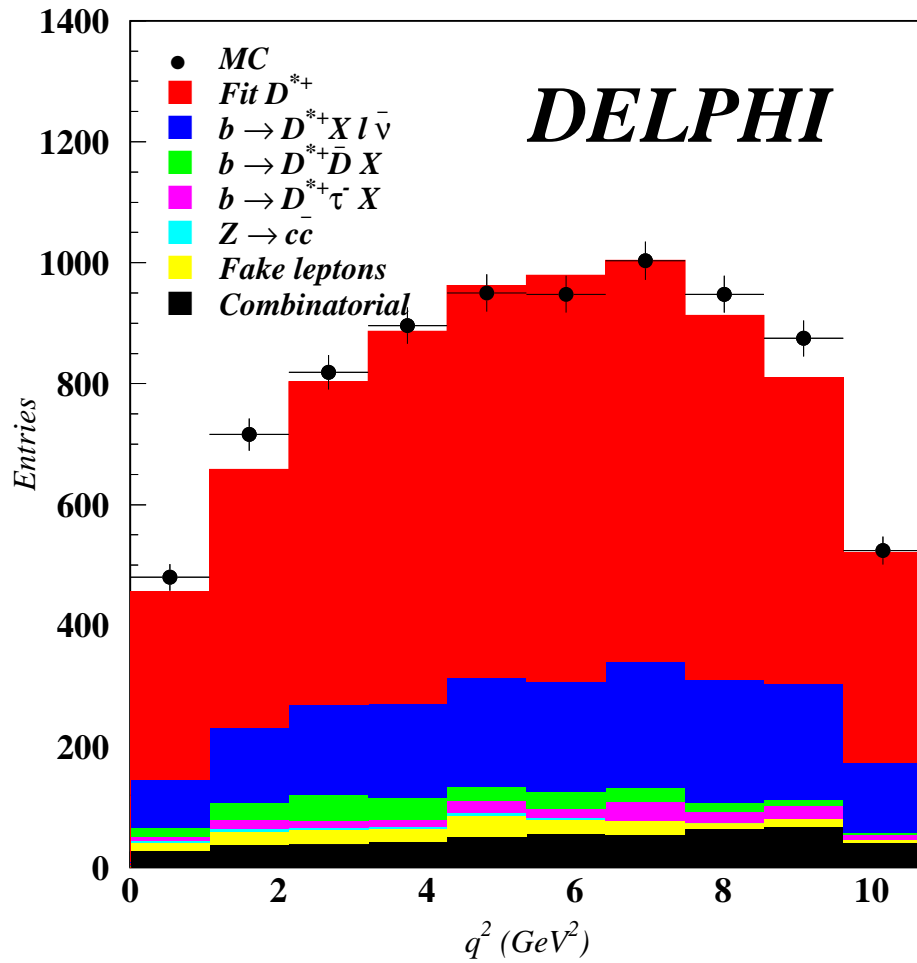
Figure 6: *Fit of MC $q\bar{q}$ and $b\bar{b}$ events. The two analysed D^0 decay channels and the two data taking periods have been combined. Only events selected within the δ_m mass interval [0.144, 0.147] GeV/c² are displayed.*
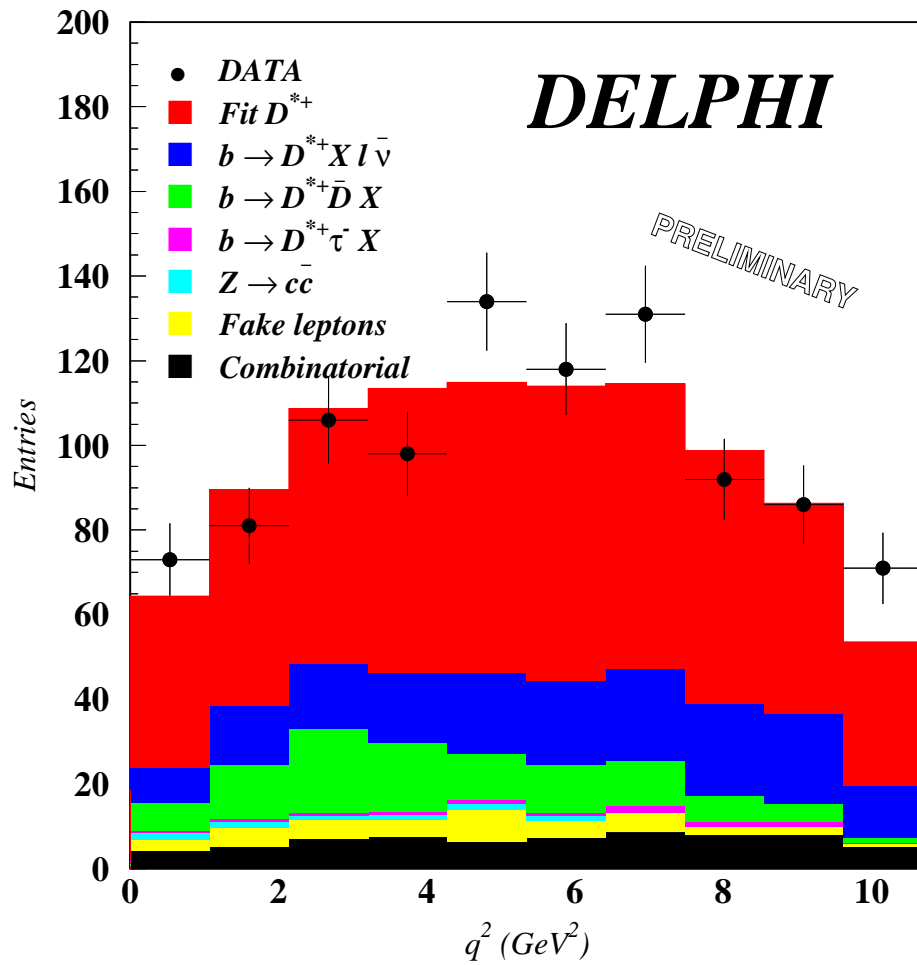
Figure 7: *Fit on real data events. All periods are combined. Only events selected within the δ_m mass interval [0.144, 0.147] GeV/c² are displayed.*

Signal (S1)	D** (S2)	Cascade (S3)	Charm (S4)	Fake lept. (S5)	τ (S6)	Comb. backg B
587 ± 24	175 ± 25	107 ± 9	9 ± 3	40 ± 6	9 ± 4	71 ± 8
	29.8 ± 4.3	18.2 ± 1.5	1.5 ± 0.5	7.8 ± 1.2	1.5 ± 0.7	8.2 ± 0.9

Table 7: *Number of events and fitted fractions (in % of signal events) attributed to the different components of the analysed sample corresponding to events selected within the δ_m mass interval [0.144, 0.147] GeV/c².*

The correlation coefficient $\rho(|V_{cb}|, \rho^2_{A_1,0})$ is equal to 0.904.

There are 998 events selected within the δ_m mass interval [0.144, 0.147] GeV/c² and the fitted fractions of the different components are given in Table 7.

Distributions for the $d_\pm$ variables, for events selected within the δ_m = [0.144, 0.147] GeV/c² interval and corresponding contributions from the fitted components are given in Figure 8.

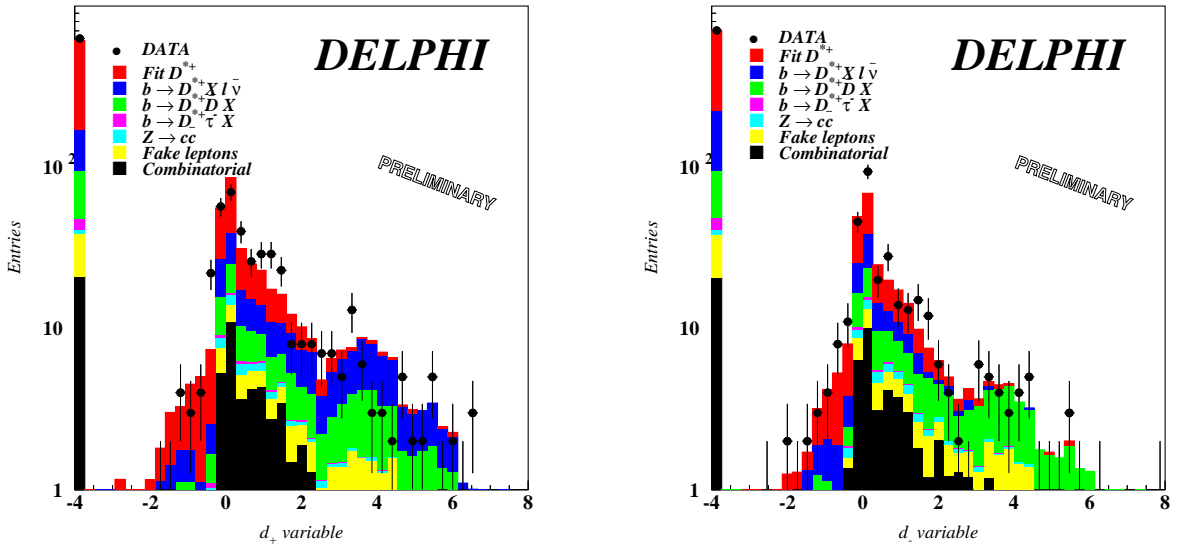Figure 8: *Distributions for the $d_\pm$ variables, for events selected within the δ_m = [0.144, 0.147] GeV/c² interval and corresponding contributions from the fitted components.*

6.3 Evaluation of systematic uncertainties

Values for the parameters taken from external measurements and hypotheses used in the present analysis have been varied within their corresponding range of uncertainty. Results are summarised in Table 8.

parameter or hypothesis	central value and uncert.	rel. err. on $\mathcal{F}_{D^*}(1)\,|V_{cb}|\ (\%)$	rel. err. on $\rho_{A_1}^2\ (\%)$	rel. err. on BR(%)
External parameters				
Rates and BR	Table 9	2.3	0.5	4.4
b-hadron frag.	see text	0.6	0.2	1.2
Detector performance				
Tracking efficiency	$\pm 0.3\%$ / track	0.7	0.2	1.3
Lepton identification	$\pm 1.5\%\ (e),\ \pm 2.0\%\ (\mu)$	0.5	0.2	1.0
Fake Lepton rates	Table 10	0.1	0.2	0.1
Resolution on q^2	see section 4	2.8	9.0	0.2
Acceptance on q^2	see section 4	1.7	5.7	0.4
Selection efficiency	Table 2	0.8	0.3	1.6
Signal modelling				
$R_1(w)$ and $R_2(w)$	[2]	0.9	22.8	-
backg. modelling				
D^{**} states	[19]	2.8	7.3	0.6
Cascade decay rate	0.0090 ± 0.0025	0.4	3.2	1.1
$\overline{B}_d^0 \to D^{*+}\tau^-\overline{\nu}_\tau X$	0.0127 ± 0.0021	0.3	0.5	0.4
$P(c \to D^{*+}X)$	0.226 ± 0.014	0.1	0.3	-
Total systematics		5.2	26.4	5.3

Table 8: *Systematic uncertainties given as relative uncertainties expressed in %.*

6.3.1 Uncertainties related to external parameters

parameter or hypothesis	central value and uncert.
R_b	0.21652 ± 0.00069
BR($D^{*+} \to D^0\pi^+$)	0.677 ± 0.005
BR($D^0 \to K^-\pi^+$)	0.0383 ± 0.0009
BR($D^0 \to K^-\pi^+\pi^+\pi^-$)	0.0749 ± 0.0031
$P(b \to \overline{B}_d^0)$	0.399 ± 0.011
$\tau(\overline{B}_d^0)$	(1.546 ± 0.021)ps

Table 9: *Values for the external parameters used in the analysis.*

Values for D and D* branching fractions into the analysed final states have been taken from [9], the value of R_b is taken from the last report of the LEPEWWG [13] whereas values for b-hadron lifetimes and production rates correspond to averaged values obtained by the LEPHF group [14]. A summary of the values used in the present analysis are given in Table 9.

Simulated events have been generated using the JETSET program with the parton shower option. The non-perturbative part of the fragmentation of b-quark jets is taken

to be a Peterson distribution which depends on a single parameter, ϵ_b:

$$D(z) = \frac{N}{z \left[1 - \frac{1}{z} - \frac{\epsilon_b}{1-z}\right]^2} \tag{27}$$

In this expression, N is a normalization factor and $z = \frac{E_B + p_{L,B}}{E_b + p_{L,b}}$, B and b indicate, respectively the B hadron and the b-quark. The average fraction of the beam energy taken by weakly decaying b-hadrons has been evaluated in [15] to be $< X_E > = \frac{<E_B>}{E_{beam}} = 0.702 \pm 0.008$. Simulated events, generated with the parameter $\epsilon_b = 0.002326$, correspond to $< X_E > = 0.7035$. The effects of a variation of the average value $< X_E >$, on the results of the analysis have been studied by weighting events generated with a known value of the variable z. To reproduce the central value and the uncertainties measured for $< X_E >$, the parameter ϵ_b has to be varied in the range: $0.00247^{+0.00080}_{-0.00067}$.

These variations on the b-quark fragmentation function induce two effects:

- a variation of the acceptance for signal events amounting to $(-0.5 \pm 1.2)\%$ in relative value,

- a variation of the resolution function on the q^2 variable. This variation comes from the fact that a correction has been applied to the fitted b-hadron energy such that it remains centreed on the simulated value independently of this value (see Section 4.5). Resolution functions have been determined on simulated weighted events to measure this effect which is found to be negligible (of the order of 0.1%).

The b-hadron lifetime used in the simulation is equal to 1.6 ps and is independent of the type of produced b-hadrons. Events have been weighted so that their lifetime is in agreement with present measurements.

6.3.2 Uncertainties from the detector performance

- Differences between simulated and real data events on the tracking efficiency have been studied in [16] and correspond to $\pm 0.3\%$ for each charged track.

- Differences between simulated and real data events on lepton identification have been measured using dedicated samples of real data events ([17]) and the RD/MC ratios are equal to $(88.5 \pm 1.5)_{92-93}\%$, $(94.0 \pm 1.5)_{94-95}\%$ for electrons. For muons, the RD/MC ratios are equal to (96% for the two periods with a $\pm 2\%$ uncertainty.

- Differences between fake lepton rates in which the lepton is a misidentified hadron, have been also measured using dedicated samples of real data events and compared with the simulation ([17]) to obtain correction factors which are summarised in Table 10.

- Resolution on the q^2 variable.

    The statistical uncertainty on the parametrization of the resolution distributions has been evaluated by varying the fitted parameters within their quoted uncertainties. The corresponding relative variations induced on fitted parameters correspond to one half of the values given in Table 8. The other half is our present estimate for effects induced by using a different parametrization of the resolution function.

22

Data set	electron	muon
92-93	0.69 ± 0.03	1.44 ± 0.03
94-95	0.77 ± 0.03	1.61 ± 0.03

Table 10: *Correction factors to apply to simulated events in which the candidate lepton is a misidentified hadron.*

The value of q^2 is obtained from the measurements of the B and D^{*+} 4-momenta (see Section 4.5). The B momentum is obtained from a constrained fit, imposing the B meson mass, which includes informations from primary and secondary vertex positions and from the energy momentum of the tracks belonging to the jet that provide an estimate for the B momentum and direction. Uncertainties on the two angles and on the momentum have been varied by 30% and new resolution distributions for q^2 have been obtained. Corresponding variations on fitted values for $\mathcal{F}_{D^*}(1)\,|V_{cb}|\,(\%)$ and $\rho_{A_1}^2$ are found to be negligible.

- The effect of a possible difference between the tuning of the b-tagging between real and simulated data events has been neglected because loose criteria have been used in this analysis.

6.3.3 Uncertainties on signal modelling

These uncertainties correspond to the use of the w dependent ratios $R_1(w)$ and $R_2(w)$ defined in Equation (7). Values for these quantities, using different models, have been obtained by the CLEO collaboration [18]: $R_1 = 1.18 \pm 0.30 \pm 0.12$, $R_2 = 0.71 \pm 0.22 \pm 0.07$ with a correlation $\rho(R_1, R_2) = -0.82$ between the uncertainties on these two measurements.

6.3.4 Uncertainties on background modelling

- The fraction of D^{*+} mesons originating from decays of D^{**} mesons depends on the total production rate of these states and on the relative fractions of the different produced states.

  Combining present measurements, the production rate of D^{*+} mesons originating from D^{**} decays and accompanied by an opposite sign lepton is [14]:

$$\mathrm{BR}(b \to D^{*+}X\ell^-\overline{\nu}_\ell) = (0.8 \pm 0.1)\% \tag{28}$$

  This information is not included in the fit as D^{*+} events produced in D^{**} decays are directly fitted on data giving:

$$\mathrm{BR}(b \to D^{*+}X\ell^-\overline{\nu}_\ell) = (0.64 \pm 0.10)\% \tag{29}$$

  which is a value compatible with the expectation given in Equation 28.

- To evaluate the effect of the uncertainty in the sample composition of produced D^{**} states, the model of [19] has been used. Parameters entering into this model have

23

been varied so that the corresponding production rates of the narrow states remain within the $\pm 1\sigma$ measured ranges defined in Equations (30, 31).

$$\mathrm{BR}(\overline{\mathrm{B}} \to \mathrm{D}_1 \ell^- \overline{\nu_\ell}) = (0.63 \pm 0.10)\% \tag{30}$$

$$\mathrm{BR}(\overline{\mathrm{B}} \to \mathrm{D}_2^* \ell^- \overline{\nu_\ell}) = (0.23 \pm 0.08)\% \text{ or } < 0.4\% \text{ at the 95\% CL} \tag{31}$$

$$\mathrm{R}^{**} = \frac{\mathrm{BR}(\overline{\mathrm{B}} \to \mathrm{D}_2^* \ell^- \overline{\nu_\ell})}{\mathrm{BR}(\overline{\mathrm{B}} \to \mathrm{D}_1 \ell^- \overline{\nu_\ell})} = 0.37 \pm 0.14 \text{ or } < 0.6 \text{ at the 95\% CL} \tag{32}$$

R^{**} is the ratio between the production rates of D_2^* and D_1 in b-meson semileptonic decays.

A dedicated simulation program has been written to generate the decay distributions of the different D^{**} states. Correlations between the leptons and hadrons momenta induced by the decay dynamics are included. The w dependence of the different form factors has been parametrized according to the model given in [19]. It has been assumed that, in addition to narrow states whose production fractions are given in Equations 30-32, broad $\mathrm{D}^* \pi$ final states, emitted in a relative S wave, are produced. The two sets of model parameters giving the two most displaced central values for the q^2 distribution are used to evaluate the systematic uncertainty coming from the sample composition of D^{**} states. These two distributions are given in Figure 9 and the fitted values obtained with these two models are given in Table 11.
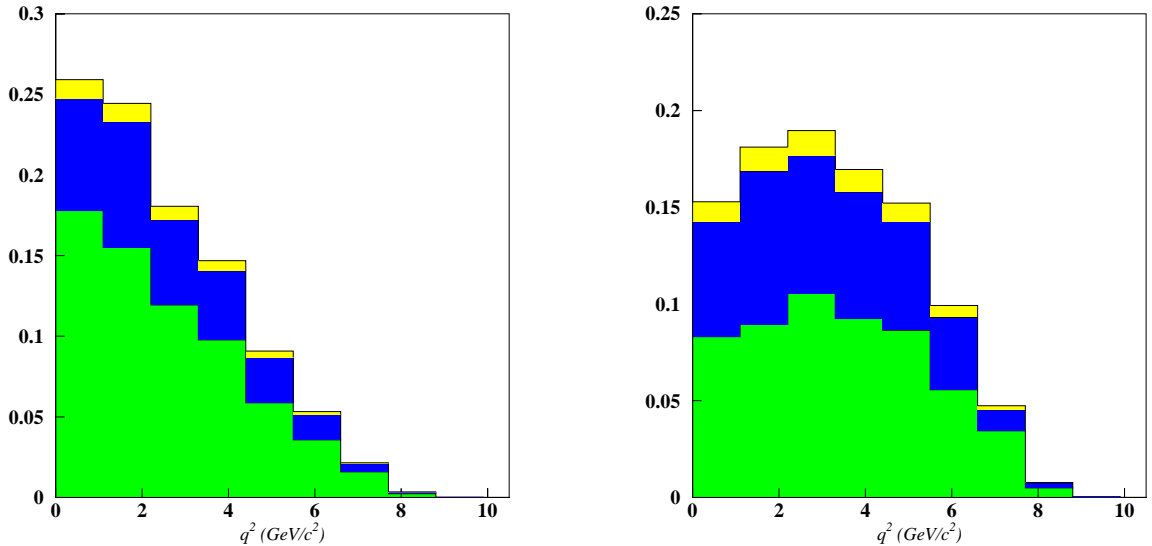

Figure 9: *q^2 distributions obtained using the two sets of parameters of the model [19], which correspond to the largest variation in the central value of these distributions and which give production rates for narrow D^{**} states that are compatible with present measurements. The three components given in each histogram correspond, from top to bottom, to narrow 2^+, narrow 1^+ and broad 1^+ states.*

	Model 1	Model 2
$\mathcal{F}_{D^*}(1)\left|V_{cb}\right|(\%)$	0.0367 ± 0.0023	0.0347 ± 0.0024
$\rho^2_{A_1}$	1.32 ± 0.20	1.14 ± 0.22
$BR(\overline{B^0_d} \to D^{*+}\ell^-\overline{\nu}_\ell)(\%)$	5.18 ± 0.27	5.12 ± 0.28

Table 11: *Fitted values corresponding to the two models describing* D^{**} *production.*

As the standard DELPHI simulation used up to now in this analysis was not based on a really justified dynamical model for D^{**} production, the average between the two results defined previously is used to determine the central values for $\mathcal{F}_{D^*}(1)\left|V_{cb}\right|(\%)$ and $\rho^2_{A_1}$. It can be noted that fitted values obtained using the modelling of D^{**} production, as given by the default DELPHI simulation, correspond to those obtained with the parameters of Model 2.

- The rate for the cascade decay background, evaluated from simulated events, has been rescaled to agree with present measurements (see Equation (17)).

- The small component of charm background events has been also evaluated using present measurements.

- The modelling uncertainty of the combinatorial component corresponding to events situated under the D^{*+} peak has a negligible contribution.

7 Conclusions

Measurements of $\mathcal{F}_{D^*}(1)\left|V_{cb}\right|$, $\rho^2_{A_1}$ and of $BR(\overline{B^0_d} \to D^{*+}\ell^-\overline{\nu}_\ell)$ have been obtained using exclusively reconstructed D^{*+} decays by the DELPHI Collaboration. Variables have been defined which allow to separate different decay mechanisms producing D^{*+} mesons in the final state. In this way the rate of D^{**} mesons has been also measured.

The following values have been obtained:

$$\mathcal{F}_{D^*}(1)\left|V_{cb}\right| = 0.0357 \pm 0.0024 \pm 0.0019; \ \rho^2_{A_1} = 1.23 \pm 0.21 \pm 0.32$$

which correspond to a branching fraction: $BR(\overline{B^0_d} \to D^{*+}\ell^-\overline{\nu}_\ell) = (5.15 \pm 0.28 \pm 0.27)\%$

These values are in agreement with previous measurements obtained by ALEPH [20], DELPHI[21] and OPAL [22] Collaborations.

References

[1] P. Abreu *et al.*, DELPHI Collaboration, Z. Phys. **C71** (1996) 539.

[2] J.E. Dubosq *et al.*, CLEO Collaboration, Phys. Rev. Lett. **76** (1996) 3898.

[3] I. Caprini, L. Lellouch and M. Neubert, Nucl. Phys. **B530** (1998) 153.

[4] C.G. Boyd, B. Grinstein and R.F. Lebed, Phys. Rev. **D56** (1997) 6895.

[5] N. Isgur and M. Wise, Phys. Lett. **B232** (1989) 113;
N. Isgur and M. Wise, Phys. Lett. **B237** (1990) 527.

[6] A. F. Falk, H. Georgi, B. Grinstein and M. B. Wise, Nucl. Phys. **B343** (1990) 1.

[7] M. Luke, Phys. Lett. **B 252** (1990) 447.

[8] T. Sjöstrand, Comp. Phys. Comm. **82** (1994)74.

[9] D.E. Groom *et al.*, Eur. Phys. J. **C15** (2000) 1.

[10] P. Abreu *et al.*, DELPHI Collaboration, Nucl. Instr. and Meth. **A378** (1996) 57.

[11] R. Barate *et al.*, ALEPH Collaboration, Eur. Phys. J. **C4** (1998) 387.

[12] A.H. Hoang, Z. Ligeti and A.V. Manohar, Phys. Rev. **D59** (1999) 074017.

[13] The LEP Collaborations ALEPH, DELPHI, L3, OPAL, the LEP Electroweak Working Group and the SLD Heavy Flavour and Electroweak Groups, A Combination of Preliminary Electoweak Measurements and Constraints on the Standard Model, prepared from contributions of the LEP and SLD experiments to the 2000 Summer conferences, CERN-EP-2001-021.

[14] Combined results on *b*-hadron production rates, lifetimes, oscillations and semileptonic decays (ALEPH, CDF, DELPHI, L3, OPAL, SLD), CERN-EP/2001-050, hep-ex/0112028.

[15] LEP/SLD Heavy Flavour Working Group, Input Parameters for the LEP Electroweak Heavy Flavour Results for Summer 1998 Conferences, LEPHF/98-01.

[16] P. Abreu *et al.*, DELPHI Collaboration, Phys. Lett. **B425** (1998) 399.

[17] K.D. Brand, I. Roncagliolo, F. Simonetto, 'Electron Identification for Electro-Weak b,c Physics', DELPHI note 96-23 PHYS 598.
P. Abreu *et al.*, DELPHI Collaboration. Eur. Phys. J **C20** (2001) 455

[18] J.E. Dubosq *et al.*, CLEO Collaboration, Phys. Rev. Lett. **76** (1996) 3898.

[19] A.K. Leibovich, Z. Ligeti, I.W. Stewart and M.B. Wise, Phys. Rev **D57** (1998) 308.

[20] D. Buskulic *et al.*, ALEPH Collaboration, Phys. Lett. **B395** (1997) 373.

[21] P. Abreu *et al.*, DELPHI Collaboration, Phys. Lett. **B510** (2001) 55.

[22] G. Abbiendi *et al.*, OPAL Collaboration, Phys. Lett. **B482** (2000) 15.